Nonstatistical Unimolecular Decay of the CH_2OO Criegee Intermediate in the Tunneling Regime

Yujie Qian[a], Thanh Lam Nguyen[b], Peter R. Franke[b], John F. Stanton[b] and Marsha I. Lester[*,a]

[a] Department of Chemistry, University of Pennsylvania, Philadelphia, PA 19104-6323, USA
[b] Department of Chemistry, University of Florida, Gainesville, FL 32611 USA

ORCID IDs
Y. Qian 0000-0001-7799-3096
T. L. Nguyen 0000-0002-7794-9439
P. R. Frank 0000-0001-9781-3179
J. F. Stanton 0000-0003-2345-9781
M. I. Lester 0000-0003-2367-3497

[*] Corresponding author email: milester@sas.upenn.edu

Abstract

Unimolecular decay of the formaldehyde oxide (CH_2OO) Criegee intermediate proceeds via a 1,3 ring-closure pathway to dioxirane and subsequent rearrangement and/or dissociation to many products including hydroxyl (OH) radicals that are detected. Vibrational activation of jet-cooled CH_2OO with two quanta of CH stretch (17-18 kcal mol^{-1}) leads to unimolecular decay at an energy significantly below the transition state barrier of 19.46 ± 0.25 kcal mol^{-1}, refined utilizing a high-level electronic structure method HEAT-345(Q)$_\Lambda$. The observed unimolecular decay rate of $1.6 \pm 0.4 \times 10^6$ s^{-1} is two orders of magnitude slower than that predicted by statistical unimolecular reaction theory using several different models for quantum mechanical tunneling. The nonstatistical behavior originates from excitation of a CH stretch vibration that is orthogonal to the heavy atom motions along the reaction coordinate and slow intramolecular vibrational energy redistribution due to the sparse density of states.

TOC Figure

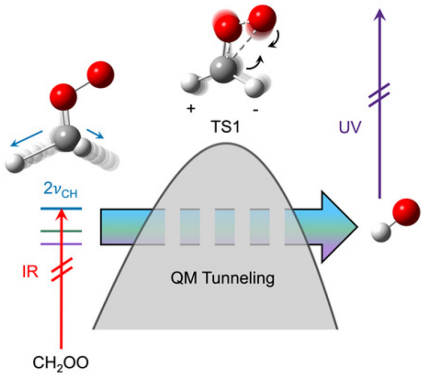

Apart from methane, alkenes are the most abundant volatile organic compounds (VOC) emitted into the troposphere and originate from various biogenic and anthropogenic sources.[1, 2] A major atmospheric removal pathway for alkenes is their reaction with ozone, a process characterized by O_3 addition across the alkene C=C bond. This reaction forms a primary ozonide (POZ), which promptly dissociates into carbonyl and zwitterionic carbonyl oxide products, the latter known as a Criegee intermediate. The unimolecular decay of the initially energized or collisionally thermalized Criegee intermediates leads to hydroxyl (OH) radicals, as well as other products, and represents a significant non-photolytic source of this key atmospheric oxidant. Alternatively, the Criegee intermediates can react with various atmospheric species, including water vapor [H_2O and $(H_2O)_2$], SO_2, NO_2, and organic acids,[3] generating more highly functionalized species that can lead to secondary organic aerosol (SOA) formation.

Formaldehyde oxide (CH_2OO), the simplest Criegee intermediate, is produced by ozonolysis of terminal alkenes, including ethylene, isoprene, and β-pinene.[4, 5] Extensive laboratory studies of CH_2OO in the past decade have been facilitated by an alternative synthetic route for generating CH_2OO via reaction of CH_2I radicals with O_2.[6] Subsequent spectroscopic studies of CH_2OO have utilized a wide range of experimental techniques including VUV photoionization[6] as well as electronic (UV),[7-9] vibrational (IR),[10] and rotational[4, 11] spectroscopies. More limited experimental studies have been conducted on the slow thermal unimolecular decay of CH_2OO.[12, 13]

This laboratory has utilized IR action spectroscopy with time-resolved UV laser-induced fluorescence (LIF) detection of the OH radical products to investigate the vibrational spectra and microcanonical unimolecular decay rates for a wide range of alkyl-substituted Criegee intermediates.[14] In these studies, unimolecular decay of Criegee intermediates proceeds by 1,4 H-atom transfer from a methyl or methylene group adjacent to the terminal oxygen, forming a vinyl hydroperoxide (VHP) that dissociates via O-O bond fission to form OH + vinoxy radicals[15-20] or undergoing a novel OH roaming pathway before dissociation.[21, 22] Recently, an analogous 1,6 H-atom transfer mechanism was shown to efficiently lead to OH products.[23] Other unimolecular decay process for Criegee intermediates include ring closure to form dioxole, which is a rapid decay pathway for specific conformers of the β-unsaturated Criegee intermediates derived from isoprene.[24, 25]

The present study examines the unimolecular decay dynamics of jet-cooled and isolated CH_2OO, again utilizing IR action spectroscopy with time-resolved detection of OH products. Unimolecular decay of CH_2OO to OH + HCO radicals can proceed via 1,3 ring-closure or a higher energy 1,3 H-shift mechanism. The 1,3 ring-closure pathway is predicted to be the dominant channel with a transition state (TS) barrier of ca. 19-21 kcal mol^{-1} (Table S1), which has been studied theoretically in depth. The 1,3 H-shift mechanism is expected to be a minor channel due to its significantly higher TS barrier (ca. 31 kcal mol^{-1}). Figure 1 shows the energy profile for CH_2OO unimolecular decay via these two channels. The

1,3 ring-closure mechanism proceeds over a substantial barrier (TS1) to dioxirane (cyc-H_2CO_2), followed by O-O ring opening via TS3 to form the methylene bis-oxy radical (•OCH_2O•). Methylene bis-oxy can then proceed via 1,2 H-migration over a low TS4 to form "hot" formic acid [HC(O)OH]*. Under collision-free conditions, hot formic acid has sufficient internal energy to fragment to H_2O + CO (-110.6 kcal mol^{-1}), H_2 + CO_2 (-121.0 kcal mol^{-1}), or HCO + OH products (-7.4 kcal mol^{-1}).[26] However, HCO + OH is predicted to be only a minor channel with low yield under thermal conditions (ca. 2%, 300 K, 1 atm).[26] The rate limiting step for unimolecular decay of CH_2OO is isomerization to dioxirane via TS1. In the alternative 1,3 H-shift pathway, CH_2OO undergoes dissociation to HCO + OH products through a significantly higher TS barrier (TS2), 31.8 kcal mol^{-1}.[26]

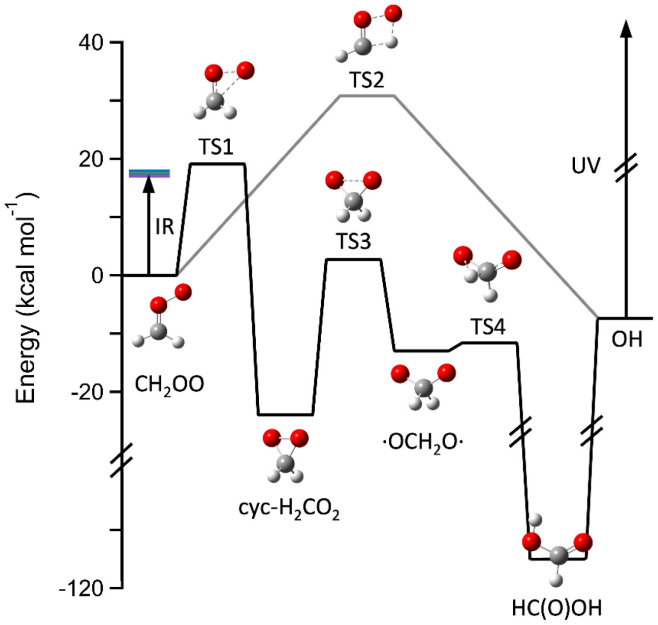

Figure 1. Energy profile for the unimolecular decay of CH_2OO Criegee intermediate to OH + HCO via 1,3 ring-closure (black line) and 1,3 H-shift (gray line) with single point energies calculated at HEAT-345(Q)$_\Lambda$. Experimentally, IR pump excitation prepares isolated and jet-cooled CH_2OO in the overtone CH stretch region ($2\nu_{CH}$), and the resultant OH products from its unimolecular decay are detected by UV probe laser-induced fluorescence (LIF) on the OH A-X (1,0) transition.

Thermal unimolecular decay of CH_2OO has been explored using various experimental methods under a range of pressure and temperature conditions. Early alkene ozonolysis studies compared the relative rate coefficients for thermal unimolecular decay of CH_2OO to that for its bimolecular reaction with SO_2,[6] obtaining upper limits for k_{uni} of $\leq 9.4 \pm 1.7$ s^{-1} (293 K, 760 Torr)[27] and ≤ 4.2 s^{-1} (298-303 K, 760 Torr),[28] which were qualitatively consistent with an early theoretical prediction of 0.3 s^{-1} at 298 K in the high pressure limit.[29] A subsequent ethene ozonolysis experiment reported k_{uni} of 0.19 ± 0.07 s^{-1} (297 K, 760 Torr), again by benchmarking against the bimolecular reaction with SO_2.[30] An upper limit for CH_2OO unimolecular decay rate of $\leq 11.6 \pm 8.0$ s^{-1} (293 K, 7-30 Torr) was obtained using the alternate synthetic

route involving photolysis of CH_2I_2 and reaction with O_2 to generate CH_2OO.[31] The most recent experimental studies were conducted at higher temperatures over a range of pressures to obtain the unimolecular decomposition rates $k(T,P)$ for stabilized CH_2OO. Stone *et al*. measured experimental decomposition rates for CH_2OO over a range of temperatures (450–650 K) and pressures (2–350 Torr), and obtained a significantly slower unimolecular decay rate of k_{uni} (298 K, 760 Torr) = $1.1^{+1.5}_{-1.1} \times 10^{-3}$ s^{-1} by extrapolation to atmospheric conditions, which agreed well with the calculated thermal rates using a TS barrier of 19.5 kcal mol^{-1}.[12] In addition, Peltola *et al.* explored the time-dependent unimolecular loss of CH_2OO over a range of temperatures (296-600 K) and pressures (5-400 Torr), in this case utilizing an alternate precursor CH_2IBr to generate CH_2OO. This study evaluated k_{uni} by extrapolation to atmospheric conditions using master-equation modeling, yielding a unimolecular decomposition rate in good accord with the values predicted using a TS barrier of 20.5 kcal mol^{-1}.[13]

In the present study, the IR action spectrum of jet-cooled and isolated CH_2OO is obtained in the overtone CH stretch region ($2\nu_{CH}$) region and compared with anharmonic vibrational frequency calculations obtained using second-order vibrational perturbation theory (VPT2).[32] IR excitation in the $2\nu_{CH}$ region provides ca. 17-18 kcal mol^{-1} of activation energy, promoting CH_2OO to energies below the theoretically predicted TS barriers for its unimolecular decay. As a result, formation of OH products from CH_2OO proceeds in the tunneling regime, specifically by tunneling associated with the 1,3 ring-closure step or the significantly higher energy 1,3 H-shift pathway. The experimental kinetic results are compared with microcanonical statistical rate calculations $k(E)$ using Rice-Ramsperger-Kassel-Marcus (RRKM) theory.[33]

In a previous paper, we used the HEAT-345(Q) method to construct a potential energy surface of (rapid) dissociation of energized CH_2OO.[26] It is fairly well established that the CCSDT(Q) method overestimates the quadruples increment to the electron correlation energy of ozone and Criegee intermediates.[34-36] This issue can be improved by using the fully iterative quadruple Q (or higher order) electron correlation method. Recent studies show that the $(Q)_\Lambda$ calculation, which is much cheaper than the full Q calculation, can provide a comparable accuracy for such a case.[37] For this reason, in this work both HEAT-345Q and HEAT-345$(Q)_\Lambda$ methods are used. As seen in Table S2, heats of formation for CH_2OO calculated with these two methods surpass that of HEAT-345(Q) and agree very well with a benchmark ATcT value.[38] In addition, the HEAT-345$(Q)_\Lambda$ calculations also yield an excellent result for the heat of formation of dioxirane. This finding suggests that HEAT-345$(Q)_\Lambda$ method is suitable for this reaction system. Unless stated otherwise, HEAT-345$(Q)_\Lambda$ results will be used for the following discussion. The ring-closure of CH_2OO to dioxirane is the rate-determining step, which needs to overcome a barrier of 19.46 kcal mol^{-1}, with a plausible uncertainty of 0.25 kcal mol^{-1}, calculated with the HEAT-345$(Q)_\Lambda$ method (see Table S3). To examine possible effects of non-dynamic electron correlation

(i.e. multireference character), MRCI+Q method was also used here to compute a barrier for the ring-closure step. The difference between the MRCI+Q and CCSDT(Q)$_\Lambda$ barriers is found to be 0.1 kcal mol^{-1} (see Table S4), which is (much) smaller than a possible uncertainty of 0.25 kcal mol^{-1}. It can be concluded that the single-reference based coupled-cluster calculations are sufficient.

Harmonic frequencies of CH_2OO, dioxirane, and the ring-closing barrier were evaluated using an *ab initio* composite scheme ("low recipe"), the precise definition of which is given elsewhere.[39] It is similar in nature to HEAT—based on all-electron CCSD(T) extrapolated to the CBS limit and including a CCSDT(Q)$_\Lambda$ correction, a scalar relativistic correction, and the Diagonal Born–Oppenheimer correction (DBOC). Anharmonic vibrational frequencies are calculated for CH_2OO using B2PLYP-D3/cc-pVTZ and CCSD(T)/ANO1 methods along with second-order vibrational perturbation theory (VPT2) as implemented in Gaussian16[40] and CFOUR[41] (Figure S1, Table S5). The B2PLYP-D3 results are utilized for IR transitions and intensities in the $2\nu_{CH}$ spectral region.

Microcanonical energy-dependent rates $k(E, J=0)$ are calculated for CH_2OO unimolecular decay via the 1,3 ring-closure and 1,3 H-shift pathways based on statistical RRKM theory and semi-classical transition state theory (SCTST) using the Master-Equation System Solver (MESS)[42] as well as Multiwell.[43] Given that $2\nu_{CH}$ excitation is lower in energy than the theoretical barriers for both pathways (see Figure 1), the reaction must take place in a classically forbidden regime by tunneling through the barrier. In this work, three different models, specifically 1D-asymmetric Eckart in MESS, multidimensional-SCTST in Multiwell, and 1D-WKB, are used to treat quantum-mechanical tunneling effects in computing $k(E)$.

The search for IR absorption bands of CH_2OO is guided by VPT2 (anharmonic) frequency calculations at the B2PLYP-D3/cc-pVTZ level of theory. Three IR transitions of CH_2OO are predicted in the overtone CH stretch region ($2\nu_{CH}$) from 5940 to 6290 cm^{-1} as shown in Figure 2, Figure S1 and Table S5, including the first overtone transitions associated with an asymmetric and a symmetric methylidene CH stretch (6273 cm^{-1}, $2\nu_1$; 5970 cm^{-1}, $2\nu_2$), and a combination transition involving asymmetric and symmetric CH stretches (6081 cm^{-1}, $\nu_1 + \nu_2$). The $2\nu_1$ transition is expected to show the strongest absorption intensity, while the $2\nu_2$ and $\nu_1 + \nu_2$ transitions are predicted to be ca. 3-fold weaker. The predicted transitions are broadened (Gaussian distribution with ca. 9 cm^{-1} FWHM) in Figure 2 to reflect the breadth of the rotational band contour anticipated under jet-cooled conditions (T_{rot} = 10 K, Figure S2).[15, 16]

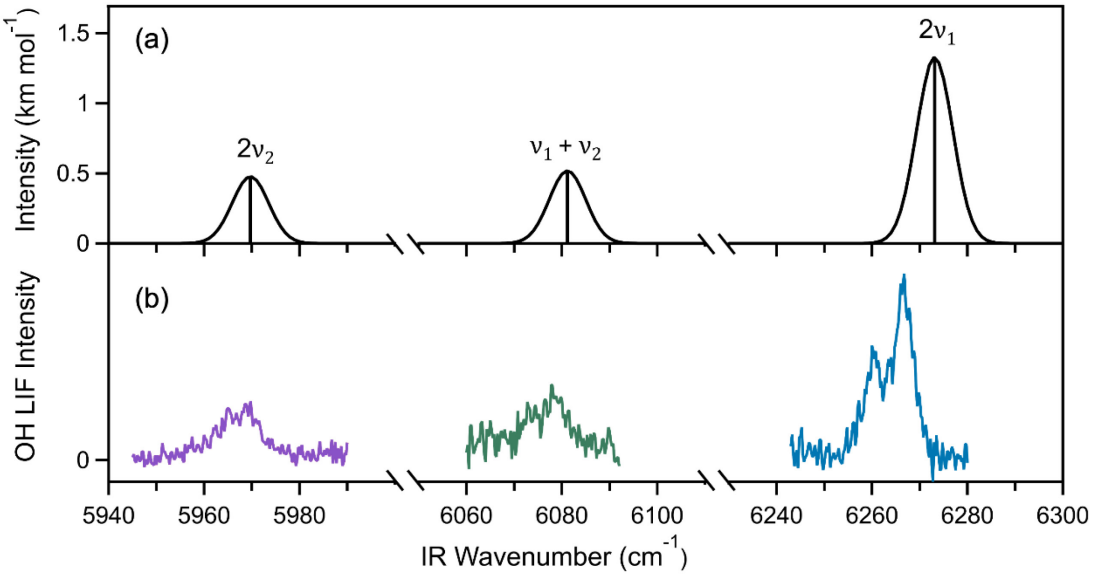

Figure 2. (a) Theoretically predicted vibrational transitions for CH_2OO in the overtone CH stretch ($2\nu_{CH}$) region at the B2PLYP-D3/cc-pVTZ level of theory. Anharmonic frequencies and intensities derived using VPT2 are shown as stick spectra and broadened to reflect the rotational band contour at ca. 10 K. (b) Experimental IR action spectral features observed for CH_2OO in the $2\nu_{CH}$ region from 5940 to 6290 cm^{-1} with UV LIF detection of OH (v=0) products.

The experiments utilize IR action spectroscopy, which depends on both IR absorption and detection of OH products, and thus differs from direct IR absorption spectroscopy. In IR action spectroscopy, the experimentally observed IR spectral features depend on both the intrinsic transition moment strength and the OH product yield arising from the IR-activated species. The experimental IR action spectrum resulting from multiple scans (scan speed of 0.025 cm^{-1} s^{-1}) is shown in Figure 2. The strongest feature observed at 6263.8 cm^{-1} (band origin, blue) with notable rotational band structure (see Figure S2) is shifted -9 cm^{-1} from the predicted $2\nu_1$ (overtone of asymmetric CH stretch) transition at 6273 cm^{-1}. Two weaker features are detected at 5967.7 cm^{-1} (purple), shifted -2 cm^{-1} from the predicted $2\nu_2$ (overtone of symmetric CH stretch) transition, and at 6075.9 cm^{-1} (green), shifted -5 cm^{-1} from the prediction for $\nu_1 + \nu_2$ (combination of symmetric and asymmetric CH stretch). The observed IR band origins and relative intensities are consistent with the theoretical calculations. The relatively weak signals observed for CH_2OO by IR action spectroscopy[15] can be attributed to a small branching fraction to OH products, in accord with theoretical predictions under thermal conditions.[12, 13, 26] The experimental IR spectral features were recorded at IR-UV time delays of 500 ns ($2\nu_1$) and 700 ns ($2\nu_2$, $\nu_1 + \nu_2$), reflecting their temporal profiles to OH products upon unimolecular decay of CH_2OO.

The temporal profile of the OH products generated upon $2\nu_1$ excitation of CH_2OO at 6266 cm^{-1} (peak of R-branch) consists of an exponential rise and fall as shown in Figure 3. The exponential rise of OH

products arises from unimolecular decay of IR-activated CH_2OO. The slower exponential fall is purely experimental in nature and results from the OH products moving out of the spatial region irradiated by the UV probe laser, which is relatively unchanged for many Criegee intermediates studied to date.[18, 19, 23, 44-46] The experimental decay rate is separately measured from vibrationally excited *syn*-CH_3CHOO at 6081 cm^{-1}, which undergoes rapid unimolecular decay to OH radicals (Figure S3, $\tau_{rise} \leq 5$ ns) upon IR excitation and gives rise to a higher signal-to-noise level compared to CH_2OO. This yielded an accurate determination of the purely experimental fall rate ($k_{fall} = 8.2 \pm 0.2 \times 10^5$ s^{-1}, $\tau_{fall} = 1.2 \pm 0.03$ μs) with $\pm 2\sigma$ uncertainty arising from repeated measurements. As described in previous publications,[18, 19, 23, 44-46] the experimental OH temporal profile is fit with a biexponential function including the convoluted IR and UV pulse widths along with the fixed k_{fall}. For CH_2OO, $2\nu_1$ activation at 6266 cm^{-1} results in the appearance of OH products with a rise rate $k_{rise} = 1.6 \pm 0.4 \times 10^6$ s^{-1} ($\tau_{rise} = 610 \pm 150$ ns). The $\pm 2\sigma$ uncertainty in k_{rise} arises primarily from uncertainty in the appearance of OH products from CH_2OO with a small contribution from the uncertainty in k_{fall}. In Figure 3, the experimental IR-induced OH signal is illustrated as a function of IR-UV time delay (t) with changing colors to visualize the changing contributions of k_{rise} and k_{fall} terms to the overall OH temporal profile. As time progresses (t = 0 – 1800 ns), a gradient shift in colors from red to blue represents the increasing contribution of k_{fall} to the temporal profile. Beyond t > 1800 ns, gray indicates that the OH temporal profile is dominated by the k_{fall} term, contributing over 95% to the overall signal.

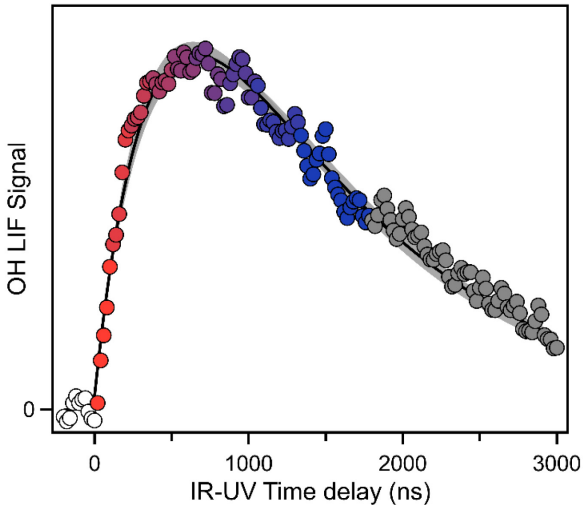

Figure 3. Temporal profile (circles) of OH products from CH_2OO unimolecular decay upon $2\nu_1$ activation at 6266 cm^{-1}. The temporal profile is fit with a dual exponential function (black line) with rise rate ($k_{rise} = 1.6 \pm 0.4 \times 10^6$ s^{-1}) resulting from unimolecular decay of CH_2OO with $\pm 2\sigma$ uncertainty (gray shade) and fall rate ($k_{fall} = 8.2 \pm 0.2 \times 10^5$ s^{-1}) arising from the OH products moving out of the UV probe volume. The change of color from red to blue to gray represents increasing contribution of the fall-off term (k_{fall}) to the overall temporal profile.

Additionally, time-dependent OH signals are observed following IR activation of the weaker $2\nu_2$ and $\nu_1 + \nu_2$ transitions at 5968 and 6076 cm^{-1}. However, the resultant IR-induced OH signals are substantially smaller, precluding a precise determination of the associated unimolecular decay rates, which are comparable or slower than that observed upon excitation to $2\nu_1$.

Statistical RRKM theory is used to compute the energy-dependent unimolecular decay rate $k(E)$ for CH_2OO under isolated jet-cooled conditions (J=0). Unimolecular decay of CH_2OO is assumed to proceed via 1,3-ring closure to dioxirane, which differs from the H-atom transfer mechanisms investigated previously for alkyl-substituted Criegee intermediates.[15, 26] The experimental IR excitation energy at 6266 cm^{-1} (17.9 kcal mol^{-1}) lies below the calculated TS barriers (TS1) ranging from 19.0 to 20.7 kcal mol^{-1} as summarized in Table S1, indicating that unimolecular decay must proceed exclusively by quantum mechanical tunneling through the barrier. The imaginary frequency ν_i at the TS is associated with a reaction coordinate including changes in the C-O-O bond angle and the H-C-O-O dihedral angle, both of which involve heavy-atom motions. Energy-dependent rates $k(E)$ are computed for 1,3-ring closure of CH_2OO to dioxirane in MESS, where quantum mechanical tunneling effects are included using an Eckart model.

Figure 4 shows the calculated microcanonical rates $k(E)$ across the 5800-7200 cm^{-1} (or 16.7-20.6 kcal mol^{-1}) energy range employing two different energy grain sizes for the density of CH_2OO reactant states (E_{grain} = 1 cm^{-1} and E_{grain} = 35 cm^{-1}, the latter corresponding to 0.1 kcal mol^{-1}) with a TS barrier of 19.46 ± 0.25 kcal mol^{-1} (HEAT-345(Q)$_\Lambda$) and ν_i of 737i cm^{-1} ("low" recipe).[39] The calculated $k(E)$ using a finer E_{grain} is a more realistic depiction of the actual kinetic behavior for CH_2OO, where $k(E)$ reveals significant fluctuations due to the sparse state density of CH_2OO across the energy range of interest. On the other hand, using a coarser E_{grain} smooths out these fluctuations, thereby representing statistical $k(E)$ values that are averages across broader energy intervals. Notably, the RRKM $k(E)$ calculations indicate a CH_2OO unimolecular decay rate that is ca. 200 times faster than the experimentally observed OH appearance rate at 6266 cm^{-1}. Although using a finer E_{grain} reduces this discrepancy, a thorough investigation of the reasons behind the disagreement between experimental and statistical theoretical results is needed.

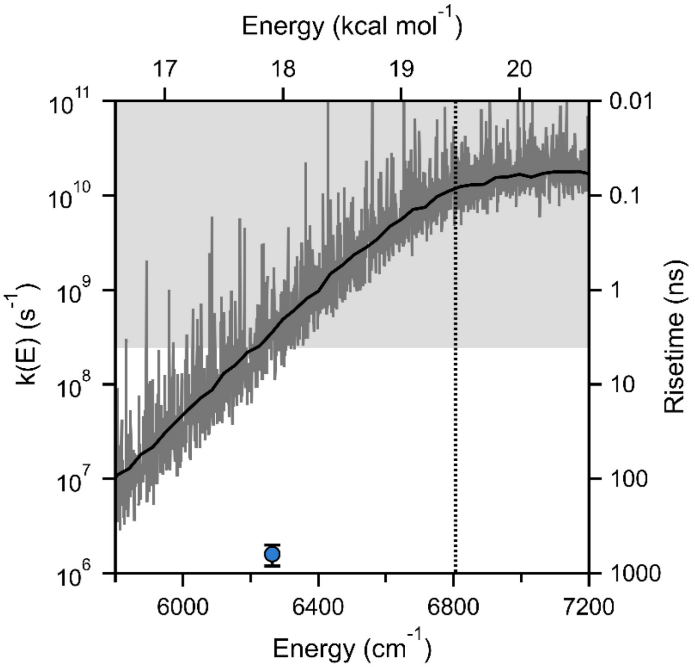

Figure 4. Statistical energy-dependent rates $k(E)$ computed for CH_2OO unimolecular decay via 1,3 ring-closure including quantum mechanical tunneling using MESS (solid lines). The fluctuation in the gray line (E_{grain} = 1 cm^{-1}) originates from the sparse state density of CH_2OO at 5800-7200 cm^{-1}, and such fluctuations are smoothed out in the black line (E_{grain} = 0.1 kcal mol^{-1}). The experimental OH appearance rate following IR excitation at 6266 cm^{-1} is shown as the blue circle with ±2σ uncertainty. The vertical dotted line represents the computed TS barrier height (19.46 kcal mol^{-1}). The gray shaded region indicates rates or lifetimes limited by the experimental time resolution (ca. 4 ns).

In addition to the Eckart model implemented in MESS, alternative approaches, specifically SCTST in Multiwell[43] and 1D-WKB (detailed in SI and Figure S4), are employed to investigate the impact of different tunneling models on the $k(E)$ rates computed for unimolecular decay of CH_2OO via 1,3 ring-closure. Using a theoretical barrier of 19.46 kcal mol^{-1} from the HEAT-345(Q)$_\Lambda$ method, the calculated $k(E)$ rates using these three models agree well (within 20-30%) with one another (Figure S5).

Intramolecular vibrational energy redistribution (IVR) is critically important in the unimolecular decay of CH_2OO as the vibrational modes that promote the 1,3 ring-closure mechanism are not directly activated by the IR excitation. Specifically, the 1,3 ring-closure process follows an intrinsic reaction path (IRC) associated with the C-O-O bend (ν_7) and CH_2 twist (ν_9), while the two vibrationally activated modes are associated with the asymmetric (ν_1) and symmetric (ν_2) CH stretches. The alternative higher energy 1,3 H-shift pathway leading directly from CH_2OO to OH products is associated with C-O-O bend (ν_7) and CH stretches, the latter of which are excited experimentally. However, the latter pathway involves a highly strained 4-membered ring structure at the TS that is ca. 12 kcal mol^{-1} higher in energy than that for ring-closure (19.46 kcal mol^{-1}), which is already significantly higher than the IR excitation energy range (17-18 kcal mol^{-1}) used in this work. The 1,3 H-shift channel is thus assumed to give

negligible contribution to the observed IR-induced OH signal.[13, 26] Therefore, intramolecular energy flow from the higher frequency CH stretches to lower frequency modes is required for unimolecular decay of CH_2OO via the 1,3 ring-closure channel.

A tier model is usually used to describe the IVR process, where vibrational energy is transferred from a specific spectroscopically prepared "bright state" to a set of near-resonant dark states, the doorway states, through anharmonic coupling. The IVR process will continue from the doorway states to a second tier with a higher density of states through weaker coupling, and this process will continue to successive tiers of bath states until the intramolecular relaxation of the initial bright state is complete. The coupling strength of the bright state to the first tier of states and potentially to higher orders of tiers determine the IVR lifetime. IVR is expected to be rapid and typically occurs on a picosecond timescale when state densities exceed about 10 states/cm^{-1}.[47, 48] However, the calculated density of states for CH_2OO shown in Figure S6 predicts ca. 1-2 states/cm^{-1} in the $2\nu_{CH}$ stretch region, which is below the threshold for IVR and could be better characterized as incomplete IVR process.[49] For vibrationally activated CH_2OO with two quanta of CH stretch, the excited bright state is not coupled to sufficient near-resonant doorway states for rapid IVR and energy redistribution is restricted by the low density of dark states. Rapid IVR is a requirement for statistical unimolecular decay as modeled using RRKM theory.

Figure 4 shows the substantial discrepancy between the experimentally observed unimolecular decay rate for CH_2OO upon $2\nu_1$ excitation and the RRKM rate predicted for 1,3 ring-closure at this energy (ca. 6260 cm^{-1}) with the Eckart tunneling model. Comparing simulated temporal profiles based on the RRKM rate with various tunneling models, $k(E) = 2.6 \times 10^8$ s^{-1} using Eckart or SCTST and 2.3×10^8 s^{-1} using WKB, with the experimental result, $k_{rise} = 1.6 \times 10^6$ s^{-1}, further illustrates the extent to which the exponential rise observed experimentally differs from the rate predicted with RRKM theory (Figure S7). The RRKM rates predicted at slightly lower energies, corresponding to $2\nu_2$ and $\nu_1 + \nu_2$ excitation, are also much more rapid than observed experimentally. Moreover, the RRKM rate predicted for the 1,3 H-shift pathway ($k(E) = 100$ s^{-1} using Eckart tunneling model) is *four orders of magnitude* slower than the experimentally observed rate at 6260 cm^{-1} (Figure S8, Table S6), primarily due to its substantially higher barrier. As a result, the 1,3 H-shift pathway is a negligible channel in the observed appearance of OH products.

RRKM theory including tunneling has yielded excellent agreement with experimental results for the unimolecular decay rates of larger Criegee intermediates via H-atom transfer.[14, 23] No mode-specific effects were observed for these larger molecules, which implies that energy from the spectroscopically activated mode is distributed statistically among near-resonant states. Additionally, the computed densities of states were significantly above the typical threshold (ca. 10 states/cm^{-1}) for complete population redistribution through IVR under jet-cooled conditions.[47, 50] IVR occurs on picosecond time

scale and is significantly faster than the unimolecular decay rates that occur on nanosecond time scales, as is required for RRKM theory.[33] However, in the present study, IVR is incomplete for vibrationally excited CH_2OO in the overtone CH stretch region due to insufficient near-resonant density of states, which leads to vastly slower IVR. The computed $k(E)$ using RRKM theory indicates that statistical unimolecular decay would occur on a few nanosecond time scale and a sub-nanosecond time scale at higher excitation energies (> 6300 cm^{-1}, Table S6). For CH_2OO ($2\nu_{CH}$), the slow IVR rate creates a bottleneck to unimolecular decay. This results in non-statistical behavior of CH_2OO excited in the $2\nu_{CH}$ region, which deviates substantially from the (tunneling-corrected) RRKM rate predicted in this study. This is analogous to the conditions that give rise to mode-specific chemistry in other small molecule systems.[51-53]

In summary, the lowest energy pathway for unimolecular decay of the CH_2OO Criegee intermediate proceeds via 1,3 ring-closure to dioxirane and subsequent rearrangement and/or dissociation to many products including hydroxyl (OH) radicals. Infrared action spectra of jet-cooled and isolated CH_2OO reveal the first overtone asymmetric ($2\nu_1$) and symmetric ($2\nu_2$) methylidene CH stretch and combination ($\nu_1+\nu_2$) transitions, and the time-resolved appearance of OH products with UV LIF detection. High-level electronic structure calculations utilizing HEAT-345(Q)$_\lambda$ refine the transition state barrier at 19.46 ± 0.25 kcal mol^{-1}, demonstrating that $2\nu_1$ excitation (6266 cm^{-1}, 17.9 kcal mol^{-1}) occurs significantly below the barrier in the tunneling regime. The unimolecular decay rate of $1.6 \pm 0.4 \times 10^6$ s^{-1} observed for CH_2OO ($2\nu_1$) is ca. 200 times slower than predicted by statistical unimolecular RRKM theory using several different models for tunneling. The nonstatistical behavior is attributed to excitation of a CH stretch vibration ($2\nu_1$), which is orthogonal to the heavy atom C-O-O (ν_7) bend and CH_2 twist (ν_9) motions along the intrinsic reaction coordinate. Moreover, intramolecular vibrational redistribution is expected to be slow due to the low density of vibrational states (1-2 states per cm^{-1}), resulting in nonstatistical unimolecular decay of CH_2OO in the tunneling regime.

Experimental Methods

A diiodomethane (CH_2I_2) precursor is heated to 40 °C, entrained in a 20% Ar/O_2 gas mixture (30 psi) and pulsed through a nozzle (1 mm orifice) and an affixed quartz capillary tube (~25 mm length, 1 mm ID) into a vacuum chamber. The cylindrically focused 355 nm output from a Nd:YAG laser (Continuum 8000, ~4 mJ $pulse^{-1}$, 10 Hz) is used to photolyze the precursor near the tip of the capillary and generate CH_2OO, which is collisionally stabilized in the capillary and cooled in the ensuing supersonic expansion. The spatially-overlapped IR-pump (~3 mm diameter, ~25 mJ $pulse^{-1}$, 2.4 ns Gaussian pulse width, 5 Hz) and UV-probe (~5 mm diameter, ~2 mJ $pulse^{-1}$, 2.4 ns Gaussian pulse width, 10 Hz) beams intersect the

stabilized CH_2OO approximately 1 cm downstream from the capillary tip in the collision-free region. The tunable IR radiation is the signal output from an optical parametric oscillator/amplifier (OPO/OPA, Laservision, 0.9 cm^{-1} bandwidth) pumped by a Nd:YAG laser (1064 nm, Continuum Surelite EX). IR excitation in the $2\nu_{CH}$ region initiates the unimolecular decay of CH_2OO to OH products, which are detected by UV laser-induced fluorescence (LIF). The UV radiation is generated by frequency doubling the output of a dye laser (Continuum ND6000) pumped by an Nd:YAG laser (532 nm, EKSPLA NL300) and is fixed on the OH $A^2\Sigma^+ - X^2\Pi_{3/2}$ (1,0) $Q_1(3.5)$ transition. OH fluorescence on the $A^2\Sigma^+ - X^2\Pi_{3/2}$ (1,1) transition is collected and detected by a gated photomultiplier tube (PMT). IR-induced OH signal is obtained by an active background subtraction scheme, which removes the background OH signal (IR-off) arising from prompt unimolecular decay of internally excited CH_2OO within the capillary and are subsequently cooled in the free jet expansion. IR-UV delay times of 500 to 700 ns are used for IR action spectra recorded in the $2\nu_{CH}$ region (5940 – 6290 cm^{-1}). The temporal appearance profile of OH products resulting from IR excitation of CH_2OO is recorded by randomly changing the delay time between IR and UV lasers.

Supporting Information Description
Additional information on stationary points, transition states, vibrational frequencies, spectral simulation, 1D-WKB tunneling, intrinsic reaction coordinate, microcanonical rates, and density of states.

Notes
The author declares no competing financial interest.

Acknowledgments
Experimental research at the University of Pennsylvania supported by the National Science Foundation under grants CHE-1955068 and CHE-2301298. Theoretical research at the University of Florida was supported by the U.S. Department of Energy, Office of Basic Energy Sciences under Award DE-SC0018164. MIL and YQ thank Stephen J. Klippenstein for helpful discussions in an early phase of this project.

References

(1) Sindelarova, K.; Granier, C.; Bouarar, I.; Guenther, A.; Tilmes, S.; Stavrakou, T.; Müller, J. F.; Kuhn, U.; Stefani, P.; Knorr, W., Global data set of biogenic VOC emissions calculated by the MEGAN model over the last 30 years. *Atmos. Chem. Phys.* **2014,** *14* (17), 9317-9341.

(2) Khan, M. A. H. S., Billie-Louise; Jenkin, M. E. S., Beth M. A. ; Moseley, K.; Walker, C.; Morris, W. C. D., Richard G. Percival, Carl J. Shallcross, Dudley E., A two-decade anthropogenic and biogenic isoprene emissions study in a London urban background and a London urban traffic site. *Atmosphere* **2018,** *9* (10), 387.

(3) Cox, R. A.; Ammann, M.; Crowley, J. N.; Herrmann, H.; Jenkin, M. E.; McNeill, V. F.; Mellouki, A.; Troe, J.; Wallington, T. J., Evaluated kinetic and photochemical data for atmospheric chemistry: Volume VII – Criegee intermediates. *Atmos. Chem. Phys.* **2020,** *20* (21), 13497-13519.

(4) Womack, C. C.; Martin-Drumel, M.-A.; Brown, G. G.; Field, R. W.; McCarthy, M. C., Observation of the simplest Criegee intermediate CH_2OO in the gas-phase ozonolysis of ethylene. *Sci. Adv.* **2015,** *1* (2), e1400105.

(5) Kroll, J. H.; Hanisco, T. F.; Donahue, N. M.; Demerjian, K. L.; Anderson, J. G., Accurate, direct measurements of oh yields from gas-phase ozone-alkene reactions using an in situ LIF Instrument. *Geophys. Res. Lett.* **2001,** *28* (20), 3863-3866.

(6) Welz, O.; Savee, J. D.; Osborn, D. L.; Vasu, S. S.; Percival, C. J.; Shallcross, D. E.; Taatjes, C. A., Direct kinetic measurements of Criegee intermediate (CH_2OO) formed by reaction of CH_2I with O_2. *Science* **2012,** *335* (6065), 204-207.

(7) Beames, J. M.; Liu, F.; Lu, L.; Lester, M. I., Ultraviolet spectrum and photochemistry of the simplest Criegee intermediate CH_2OO. *J. Am. Chem. Soc.* **2012,** *134* (49), 20045-20048.

(8) Sheps, L., Absolute ultraviolet absorption spectrum of a Criegee intermediate CH_2OO. *J. Phys. Chem.* **2013,** *4* (24), 4201-4205.

(9) Ting, W.-L.; Chen, Y.-H.; Chao, W.; Smith, M. C.; Lin, J. J.-M., The UV absorption spectrum of the simplest Criegee intermediate CH_2OO. *Phys. Chem. Chem. Phys.* **2014,** *16* (22), 10438-10443.

(10) Su, Y.-T.; Huang, Y.-H.; Witek, H. A.; Lee, Y.-P., Infrared absorption spectrum of the simplest Criegee intermediate CH_2OO. *Science* **2013,** *340* (6129), 174-176.

(11) Nakajima, M.; Endo, Y., Communication: Determination of the molecular structure of the simplest Criegee intermediate CH_2OO. *J. Chem. Phys.* **2013,** *139* (10), 101103.

(12) Stone, D.; Au, K.; Sime, S.; Medeiros, D. J.; Blitz, M.; Seakins, P. W.; Decker, Z.; Sheps, L., Unimolecular decomposition kinetics of the stabilised Criegee intermediates CH_2OO and CD_2OO. *Phys. Chem. Chem. Phys.* **2018,** *20* (38), 24940-24954.

(13) Peltola, J.; Seal, P.; Inkilä, A.; Eskola, A., Time-resolved, broadband UV-absorption spectrometry measurements of Criegee intermediate kinetics using a new photolytic precursor: unimolecular decomposition of CH_2OO and its reaction with formic acid. *Phys. Chem. Chem. Phys.* **2020,** *22* (21), 11797-11808.

(14) Stephenson, T. A.; Lester, M. I., Unimolecular decay dynamics of Criegee intermediates: Energy-resolved rates, thermal rates, and their atmospheric impact. *Int. Rev. Phys. Chem.* **2020,** *39* (1), 1-33.

(15) Liu, F.; Beames, J. M.; Petit, A. S.; McCoy, A. B.; Lester, M. I., Infrared-driven unimolecular reaction of CH_3CHOO Criegee intermediates to OH radical products. *Science* **2014,** *345* (6204), 1596-1598.

(16) Liu, F.; Beames, J. M.; Lester, M. I., Direct production of OH radicals upon CH overtone activation of $(CH_3)_2COO$ Criegee intermediates. *J. Chem. Phys.* **2014,** *141* (23), 234312.

(17) Fang, Y.; Liu, F.; Klippenstein, S. J.; Lester, M. I., Direct observation of unimolecular decay of CH_3CH_2CHOO Criegee intermediates to OH radical products. *J. Chem. Phys.* **2016,** *145* (4), 044312.

(18) Barber, V. P.; Pandit, S.; Green, A. M.; Trongsiriwat, N.; Walsh, P. J.; Klippenstein, S. J.; Lester, M. I., Four-carbon Criegee intermediate from isoprene ozonolysis: methyl vinyl ketone oxide synthesis, infrared spectrum, and OH production. *J. Am. Chem. Soc.* **2018,** *140* (34), 10866-10880.
(19) Barber, V. P.; Hansen, A. S.; Georgievskii, Y.; Klippenstein, S. J.; Lester, M. I., Experimental and theoretical studies of the doubly substituted methyl-ethyl Criegee intermediate: Infrared action spectroscopy and unimolecular decay to OH radical products. *J. Chem. Phys.* **2020,** *152* (9), 094301.
(20) Lester, M. I.; Klippenstein, S. J., Unimolecular decay of Criegee intermediates to OH radical products: prompt and thermal decay processes. *Acc. Chem. Res.* **2018,** *51* (4), 978-985.
(21) Liu, T.; Elliott, S. N.; Zou, M.; Vansco, M. F.; Sojdak, C. A.; Markus, C. R.; Almeida, R.; Au, K.; Sheps, L.; Osborn, D. L.; Winiberg, F. A. F.; Percival, C. J.; Taatjes, C. A.; Caravan, R. L.; Klippenstein, S. J.; Lester, M. I., OH roaming and beyond in the unimolecular decay of the methyl-ethyl-substituted Criegee intermediate: observations and predictions. *J. Am. Chem. Soc.* **2023,** *145* (35), 19405-19420.
(22) Taatjes, C. A.; Liu, F.; Rotavera, B.; Kumar, M.; Caravan, R.; Osborn, D. L.; Thompson, W. H.; Lester, M. I., Hydroxyacetone production from C3 Criegee intermediates. *J. Phys. Chem. A* **2017,** *121* (1), 16-23.
(23) Hansen, A. S.; Qian, Y.; Sojdak, C. A.; Kozlowski, M. C.; Esposito, V. J.; Francisco, J. S.; Klippenstein, S. J.; Lester, M. I., Rapid allylic 1,6 H-atom transfer in an unsaturated Criegee intermediate. *J. Am. Chem. Soc.* **2022,** *144* (13), 5945-5955.
(24) Vereecken, L.; Novelli, A.; Taraborrelli, D., Unimolecular decay strongly limits the atmospheric impact of Criegee intermediates. *Phys. Chem. Chem. Phys.* **2017,** *19* (47), 31599-31612.
(25) Caravan, R. L.; Vansco, M. F.; Lester, M. I., Open questions on the reactivity of Criegee intermediates. *Commun. Chem.* **2021,** *4* (1), 44.
(26) Nguyen, T. L.; Lee, H.; Matthews, D. A.; McCarthy, M. C.; Stanton, J. F., Stabilization of the simplest Criegee intermediate from the reaction between ozone and ethylene: a high-level quantum chemical and kinetic analysis of ozonolysis. *J. Phys. Chem. A* **2015,** *119* (22), 5524-5533.
(27) Berndt, T.; Voigtländer, J.; Stratmann, F.; Junninen, H.; Mauldin Iii, R. L.; Sipilä, M.; Kulmala, M.; Herrmann, H., Competing atmospheric reactions of CH_2OO with SO_2 and water vapour. *Phys. Chem. Chem. Phys.* **2014,** *16* (36), 19130-19136.
(28) Newland, M. J.; Rickard, A. R.; Alam, M. S.; Vereecken, L.; Muñoz, A.; Ródenas, M.; Bloss, W. J., Kinetics of stabilised Criegee intermediates derived from alkene ozonolysis: reactions with SO_2, H_2O and decomposition under boundary layer conditions. *Phys. Chem. Chem. Phys.* **2015,** *17* (6), 4076-4088.
(29) Olzmann, M.; Kraka, E.; Cremer, D.; Gutbrod, R.; Andersson, S., Energetics, kinetics, and product distributions of the reactions of ozone with ethene and 2,3-dimethyl-2-butene. *J. Phys. Chem. A* **1997,** *101* (49), 9421-9429.
(30) Berndt, T.; Kaethner, R.; Voigtländer, J.; Stratmann, F.; Pfeifle, M.; Reichle, P.; Sipilä, M.; Kulmala, M.; Olzmann, M., Kinetics of the unimolecular reaction of CH_2OO and the bimolecular reactions with the water monomer, acetaldehyde and acetone under atmospheric conditions. *Phys. Chem. Chem. Phys.* **2015,** *17* (30), 19862-19873.
(31) Chhantyal-Pun, R.; Davey, A.; Shallcross, D. E.; Percival, C. J.; Orr-Ewing, A. J., A kinetic study of the CH_2OO Criegee intermediate self-reaction, reaction with SO_2 and unimolecular reaction using cavity ring-down spectroscopy. *Phys. Chem. Chem. Phys.* **2015,** *17* (5), 3617-3626.
(32) Mills, I. M., Vibration-rotation structure in asymmetric-and symmetric-top molecules. *Molecular spectroscopy: Modern Research.* Academic Press, **1972,** *1*, 115-140.
(33) Baer, T.; Hase, W. L., *Unimolecular reaction dynamics: theory and experiments*. Oxford University Press, **1996.**
(34) Begley, J. M.; Aroeira, G. J. R.; Turney, J. M.; Douberly, G. E.; Schaefer, H. F., III, Enthalpies of formation for Criegee intermediates: A correlation energy convergence study. *J. Chem. Phys.* **2023,** *158* (3), 034302.

(35) Eriksen, J. J.; Matthews, D. A.; Jørgensen, P.; Gauss, J., Communication: The performance of non-iterative coupled cluster quadruples models. *J. Chem. Phys.* **2015,** *143* (4), 041101.
(36) Eriksen, J. J.; Matthews, D. A.; Jørgensen, P.; Gauss, J., Assessment of the accuracy of coupled cluster perturbation theory for open-shell systems. II. Quadruples expansions. *J. Chem. Phys.* **2016,** *144* (19), 194103.
(37) Semidalas, E.; Karton, A.; Martin, J. M. L., W4Λ: Leveraging Λ coupled-cluster for accurate computational thermochemistry approaches. *J. Phys. Chem. A* **2024,** *128* (9), 1715-1724.
(38) Ruscic, B.; Bross, D. H., Active Thermochemical Tables (ATcT) values based on ver. 1.130 of the Thermochemical Network. Argonne National Laboratory, Lemont, Illinois **2023**; ATcT.anl.gov [DOI: 10.17038/CSE/1997229] (accessed 2023-08-01).
(39) Franke, P. R.; Stanton, J. F., Rotamers of methanediol: composite ab initio predictions of structures, frequencies, and rovibrational constants. *J. Phys. Chem. A* **2023,** *127* (4), 924-937.
(40) Frisch, M. e.; Trucks, G.; Schlegel, H.; Scuseria, G.; Robb, M.; Cheeseman, J.; Scalmani, G.; Barone, V.; Petersson, G.; Nakatsuji, H., *Gaussian 16.* Gaussian, Inc. Wallingford, CT: **2016**. https://gaussian.com/gaussian16/ (accessed 2020-01-01).
(41) Matthews, D. A.; Cheng, L.; Harding, M. E.; Lipparini, F.; Stopkowicz, S.; Jagau, T.-C.; Szalay, P. G.; Gauss, J.; Stanton, J. F., Coupled-cluster techniques for computational chemistry: The CFOUR program package. *J. Chem. Phys.* **2020,** *152* (21), 214108.
(42) Georgievskii, Y.; Klippenstein, S. J. *MESS*. 2016.3.23: Argonne National Laboratory, **2016**. https://tcg.cse.anl.gov/papr/codes/mess.html (accessed 2021-05-01).
(43) J. R. Barker, T. L. N., J. F. Stanton, C. Aieta, M. Ceotto, F. Gabas, T. J. D. Kumar, C. G. L. Li, L. L. Lohr, A. Maranzana, N. F. Ortiz, J. M. Preses, J. M. Simmie, J. A. Sonk, and P. J. Stimac *Multiwell*, MultiWell-<2019> Software Suite University of Michigan, Ann Arbor, MI, **2019**. https://multiwell.engin.umich.edu (accessed 2022-01-01).
(44) Fang, Y.; Barber, V. P.; Klippenstein, S. J.; McCoy, A. B.; Lester, M. I., Tunneling effects in the unimolecular decay of $(CH_3)_2COO$ Criegee intermediates to OH radical products. *J. Chem. Phys.* **2017,** *146* (13), 134307.
(45) Fang, Y.; Liu, F.; Barber, V. P.; Klippenstein, S. J.; McCoy, A. B.; Lester, M. I., Deep tunneling in the unimolecular decay of CH_3CHOO Criegee intermediates to OH radical products. *J. Chem. Phys.* **2016,** *145* (23), 234308.
(46) Hansen, A. S.; Bhagde, T.; Qian, Y.; Cavazos, A.; Huchmala, R. M.; Boyer, M. A.; Gavin-Hanner, C. F.; Klippenstein, S. J.; McCoy, A. B.; Lester, M. I., Infrared spectroscopic signature of a hydroperoxyalkyl radical (•QOOH). *J. Chem. Phys.* **2021,** *156* (1), 014301.
(47) Lehmann, K.; Scoles, G.; Pate, B., Intramolecular dynamics from eigenstate-resolved infrared spectra. *Annu. Rev. Phys. Chem.* **1994,** *45* (1), 241-274.
(48) Kim, H. L.; Kulp, T. J.; McDonald, J. D., Infrared fluorescence study on the threshold of intramolecular vibrational state mixing. *J. Chem. Phys.* **1987,** *87* (8), 4376-4382.
(49) Felker, P. M.; Zewail, A. H., Dynamics of intramolecular vibrational-energy redistribution (IVR). I. Coherence effects. *J. Chem. Phys.* **1985,** *82* (7), 2961-2974.
(50) Yoo, H. S.; DeWitt, M. J.; Pate, B. H., Vibrational dynamics of terminal acetylenes: I. Comparison of the intramolecular vibrational energy redistribution rate of gases and the total relaxation rate of dilute solutions at room temperature. *J. Phys. Chem. A* **2004,** *108* (8), 1348-1364.
(51) Crim, F. F., Bond-Selected Chemistry: Vibrational state control of photodissociation and bimolecular reaction. *J. Phys. Chem.* **1996,** *100* (31), 12725-12734.
(52) Zare, R. N., Laser control of chemical reactions. *Science* **1998,** *279* (5358), 1875-1879.
(53) Crim, F. F., Chemical dynamics of vibrationally excited molecules: Controlling reactions in gases and on surfaces. *Proc. Natl. Acad. Sci.* **2008,** *105* (35), 12654-12661.